5. Magneto-optic Kerr effect on Fe/Tb multilayers

As explained above the structural and magnetic properties of Fe/Tb MLs is strongly influenced by the preparation conditions. In addition, the crystallization behavior of the Fe layers is determined by the individual Fe thickness. In this Chapter effects of different substrate temperature on morphological, magnetic and magneto-optic properties of Fe/Tb MLs are described, which were studied by using the polar Kerr ellipticity, ε_K, at temperatures, $50 \leq T \leq 300$ K. In the first section the influence of the Fe thickness on the structural phase transition from amorphous to crystalline Fe with increasing t_{Fe} and on the PMA investigated on the Fe/Tb MLs with variant Fe and constant Tb layer thickness, $t_{Fe} = 1 – 5$ and $t_{Tb} = 1.9$ nm, at RT will be shown [Kim95].

In the second section the analysis of the Kerr hysteresis loops obtained at temperatures $50 \leq T \leq 300$ K, their decomposition into individual components and fitting of the saturation Kerr ellipticity by using power laws will be discussed. In particular the existence of different amorphous Fe modifications, a-Fe encountered for $t_{Fe} \leq 3.0$ and 2.5 nm in LT and HT MLs, respectively, and a small fraction of magnetically uncoupled a-Fe at all temperatures, will be shown and their magnetic and MO properties, their influence on the shape of the ε_K hysteresis loops will be presented. Particularly a transition from Fe-dominated interface PMA to Tb-dominated bulk PMA with extreme coercivity, $H_c > 4$ MA/m, and field-induced effects on the peculiar hysteresis cycles in the crossover range $160 < T < 210$ K observed in LT MLs with thick a-Fe layers, $t_{Fe} = 3$ nm, will be discussed in detail.

5.1. Thickness dependence

Fig. 5.1 shows the polar Kerr ellipticity (ε_K) curves of the Fe/Tb MLs with fixed Tb thickness, $t_{Tb} = 1.9$ nm, and variant Fe thicknesses, $t_{Fe} = 1.5$, 3.0 and 5.0 nm. They were obtained at room temperature (RT) after preparation at „low“ and „high“ substrate temperatures, $T_s = 150$ K (LT, Fig. 5.1a) and 300 K (HT, Fig. 5.1b). A first glance at the hysteresis curves thus obtained immediately shows that they do not only depend strongly on the thickness t_{Fe}, but also on T_s. The HT hysteresis loops (Fig. 5.1b) reveal complex structures, which strongly differ from the

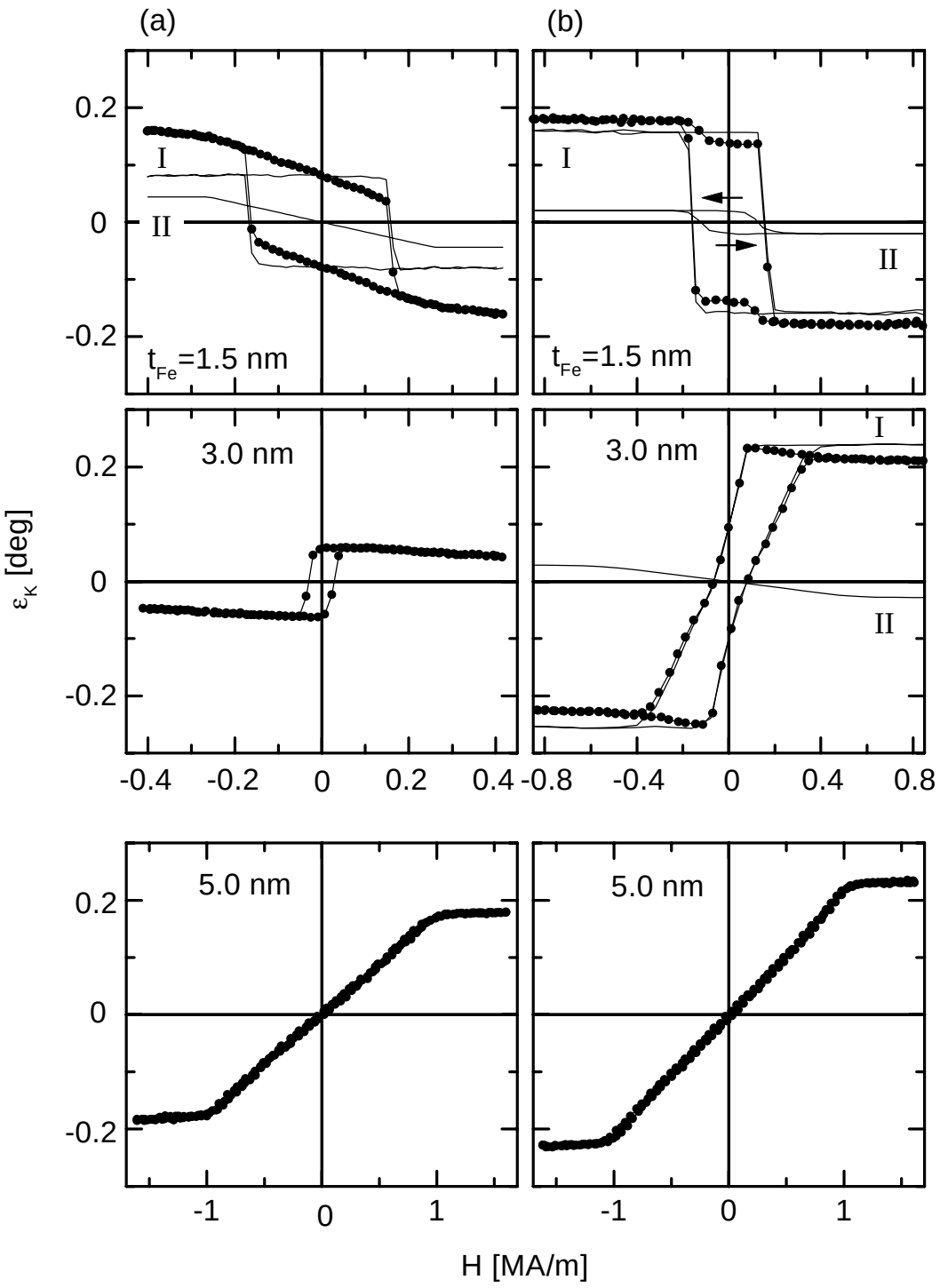

Fig. 5.1: Polar Kerr ellipticity (ε_K) hysteresis loops of the Fe/Tb multilayers with fixed Tb thickness t_{Tb} = 1.9 nm and variant Fe thicknesses, t_{Fe} = 1.5, 3.0 and 5.0 nm, obtained at room temperature and a light wavelength λ = 633 nm. The samples are evaporated at different substrate temperatures, T_s = 150 (a; LT) and 300 K (b; HT). The decomposed individual components (see text) are denoted as curves I and II.

more uniform ones obtained on the LT MLs (Fig. 5.1a). As will be discussed below this is connected with structural heterogeneity of the MLs involving different modifications of Fe and interface alloying of Fe with Tb [Kim98a].

There are also common properties observed both on LT and HT MLs. In both series the sign of the MOKE signal changes in the range $1.5 \leq t_{Fe} \leq 2.0$ nm. This is attributed to a change of orientation of the magnetic moments of the iron layers, m_{Fe}, with respect to the applied field. Since the MOKE signal of TM/RE systems at visible wavelengths is primarily due to the TM component [Chal90] and ferrimagnetic coupling is encountered in the case of Fe/Tb [Carb90], a change of sign in ε_K signifies the occurrence of a compensation point. Thick enough Fe layers, $t_{Fe} \geq 2$ nm, ensure their magnetic dominance, $m_{Fe} > m_{Tb}$, where m_{Tb} is the magnetic moment of the Tb layers. For $t_{Fe} \leq 1.5$ nm, however, Tb dominates at RT. Similar dependencies were observed on Fe/Tb MLs prepared by sputtering techniques [Pier91]. Another common property referring to both LT and HT MLs is their changeover from PMA to in-plane anisotropy in the interval $3.0 < t_{Fe} < 5.0$ nm. This is clearly reflected by the change from rectangular and hysteretic to oblique and reversible magnetization loops, where saturation is achieved at $H_s \approx 1$ MA/m in the latter case.

Some correlations between the magneto-optic and the magnetic properties of the LT MLs (Fig. 5.1a) are illustrated in Fig. 5.2, where the saturated MOKE ellipticity, ε_K^s (a), and the corresponding saturation field, H_s (b), are plotted versus t_{Fe}. In both plots three regions can be distinguished. For $t_{Fe} \leq 3$ nm (region I) fairly low values of both ε_K^s and H_s are encountered. According to CEMS measurements [Rich95], the MLs in the region I contain amorphous Fe, a-Fe. On the other hand, for $t_{Fe} \geq 4.0$ nm (region III) typical values of $\varepsilon_K^s \approx 0.2°$ and $H_s \approx$ 1MA/m of crystalline Fe, α-Fe, are observed [Kim98a, b]. In the changeover range, $3.0 \leq t_{Fe} \leq$ 4.0 nm (region II), a heterogeneous structure of the Fe films might be anticipated. Although crystallization of Fe takes place above the critical film thickness, $t_{Fe}^{cr} \approx 3.0$ nm, a certain percentage of Fe remains amorphous [Dufo91]. CEMS reveals a fraction of 84% a-Fe in the sample with $t_{Fe} = 3.5$ nm from our LT series [Rich95]. Its relative importance becomes negligible as $t_{Fe} > 4$ nm, i. e. in region III.

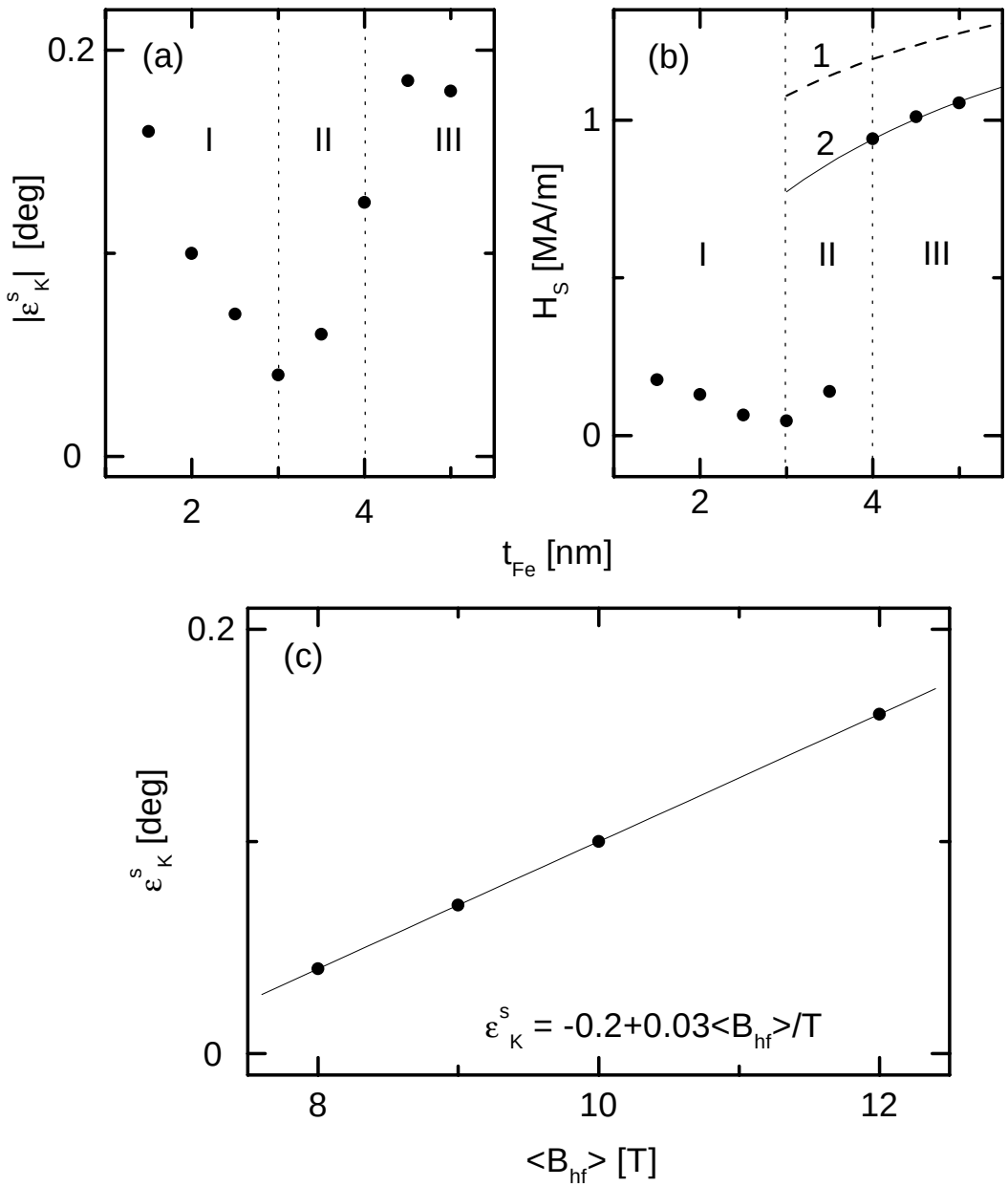

Fig. 5.2: Correlations between magneto-optic and magnetic properties of LT multilayers (Fig. 5.1a): saturated polar Kerr ellipticity, ε^s_K(a), and corresponding saturation magnetic field, H_s(b), versus thickness of the Fe layers, t_{Fe}, and (c): linear relationship between average hyperfine field <B_{hf}> [Rich95] and ε^s_K. Curves 1 and 2 (b: dashed and solid lines) show model calculations of H_s vs. t_{Fe} taking into account interface thicknesses, $t_{a\text{-}FeTb}$ = 0 and 0.85 nm, respectively.

Surprisingly, ε^s_K decreases with increasing t_{Fe} in region I (Fig. 5.2a), although one rather expects a linear increase in the ultrathin film limit [Višn95]. Obviously this tendency is

counteracted by a simultaneous decrease of the saturation magnetization, M^s_{Fe}, at the given measurement temperature, RT. This is a consequence of the well-known [Hond93] decrease of the ordering temperature of Fe/Tb MLs with increasing t_{Fe} provided that they involve magnetic interfaces (consisting of amorphous FeTb alloys) and non-magnetic a-Fe (at RT!) in their central regions. This structure has been confirmed by probe layer CEMS measurements on our LT ML series referring to region I in Fig. 5.2a and b [Rich96a]. As a consequence, also the average hyperfine field, $<B_{hf}>$, at the Fe nuclei decreases with increasing t_{Fe}. We find a linear relationship (Fig. 5.2c) between $<B_{hf}>$ and the saturated MOKE signals,

$$\varepsilon_K^s = -0.2 + 0.03 < B_{hf} > /\mathrm{T}\,. \qquad (5.1)$$

A similar relationship was reported on sputtered Fe/Tb MLs in the ultrathin limit, $t_{Fe} < 2.3$ nm [Fnid93].

In parallel with the decrease of ε_K^s the saturation field H_s decreases significantly with increasing t_{Fe} in region I (Fig. 5.2b). It shows a proportionality between H_s and the magnetization of the Fe layers. In the crossover region II the saturation field steeply rises and attains a value $H_s \approx 1.05$ MA/m in the region III at $t_{Fe} = 5$ nm (Fig. 5.2b). This value is to be compared with that obtained for bulk thin films of α-Fe, which exhibit $H_s = M^s_{\alpha\text{-Fe}} = 1.76$ MA/m owing to the dominating shape anisotropy and the demagnetization factor $N_\perp = 1$. Two effects are responsible for the reduction of H_s by 38% in the Fe/Tb MLs. First, the total volume, $V = V_{Fe} + V_{Tb}$, which determines the magnetization, is enhanced by the volume of non-magnetic Tb and thus decreases the ratio, $M = m/V < M^s_{\alpha\text{-Fe}}$. Hence the magnetization of the Tb/Fe MLs is decreased as presented in Fig. 5.2b by a broken line labeled as 1. Second, by assuming interfaces with virtually vanishing moments and inserting constant thicknesses the observed variation of H_s vs. t_{Fe} can nearly perfectly be modeled with $t_{a\text{-FeTb}} = 0.85$ nm (Fig. 5.2b, curve 2). This result corroborates inferences made in previous investigations [Cher91, Scho94a, Kim98a and b].

The complicated structure of the ε_K^s vs. H curves obtained on the HT MLs with $t_{Fe} = 1.5$ nm and 3.0 nm (Fig. 5.1b) can be decomposed into individual components as shown by solid lines denoted as I and II. Let us first discuss the leading contributions, I. They form rectangular and parallelogram shaped loops for $t_{Fe} = 1.5$ and 3.0 nm, respectively. According to CEMS measurements [Rich95] in both cases strong PMA is encountered as indicated by spin texture

angles $<\theta> \approx 11°$ with respect to the ML normal. However, structural differences are encountered, since the low-t_{Fe} sample turns out to be amorphous, whereas above t_{Fe} = 2.0 nm crystalline α-Fe forms [Dufo91]. Obviously, a coherent rotation model seems applicable to the former case, whereas for t_{Fe} = 3.0 nm the magnetization reversal probably occurs via domain formation. This is a consequence of the larger magnetization involved and the enhancement of the demagnetization energy, $\mu_0 (M^s_{\alpha-Fe})^2 / 2$, and explains the fairly low remanence, $\varepsilon^r_K (H=0) \approx 0.4\, \varepsilon^s_K$.

The second components, II, are inverted in sign, and reveal virtually vanishing hysteresis and fairly low saturation fields, $H_s \approx 0.4$ MA/m. Most remarkably, they are nearly identical in both cases, (1) and (2). Hence we are inclined to assume a common origin, to be found in the morphology of the MLs. As discussed in a previous study devoted to Fe/Tb MLs containing diamagnetic blocking layers of Ag [Kim98b] this novel component reveals soft magnetic behavior without hysteresis and seems to be magnetically decoupled from the bulk of the layers. Its Kerr spectroscopic weight appears considerably enhanced in the near infrared spectral region [Kim98b]. Further examples of such heterogeneous hysteresis curves will be discussed in the following chapter.

5.2. Temperature dependencies

5.2.1. HT multilayers (T_s = 300 K)

Fig. 5.3 shows the variation with decreasing temperature of the hysteresis loops referring to the HT MLs with t_{Fe} = 1.5 (a, b) and 3.0 nm (c, d). The curves labeled as 1 (T = 300 K) correspond to those displayed in Fig. 5.1b. The most prominent feature is the tremendous increase of their width (=$2H_s$) by a factor of approximately 20 when cooling from 300 (1) to 50 K (4). Furthermore, the sharp switching behavior at $\pm H_s$ of the loops becomes more perfect upon cooling in both cases. Both features are consequences of increasing PMA due to the increasing polarization of Tb at decreasing T (the Curie temperature of pure Tb is T_c = 219 K) [Elli72]. In parallel, the amplitudes ε^s_K are increasing by factors of approximately 2 and 1.3 between 300 and 50 K for t_{Fe} = 1.5 and 3.0 nm, respectively. As will be discussed in more

detail below this behavior is related to the temperature dependence of the saturation magnetization of the Fe layers, $M^s_{Fe} \propto \varepsilon^s_K$.

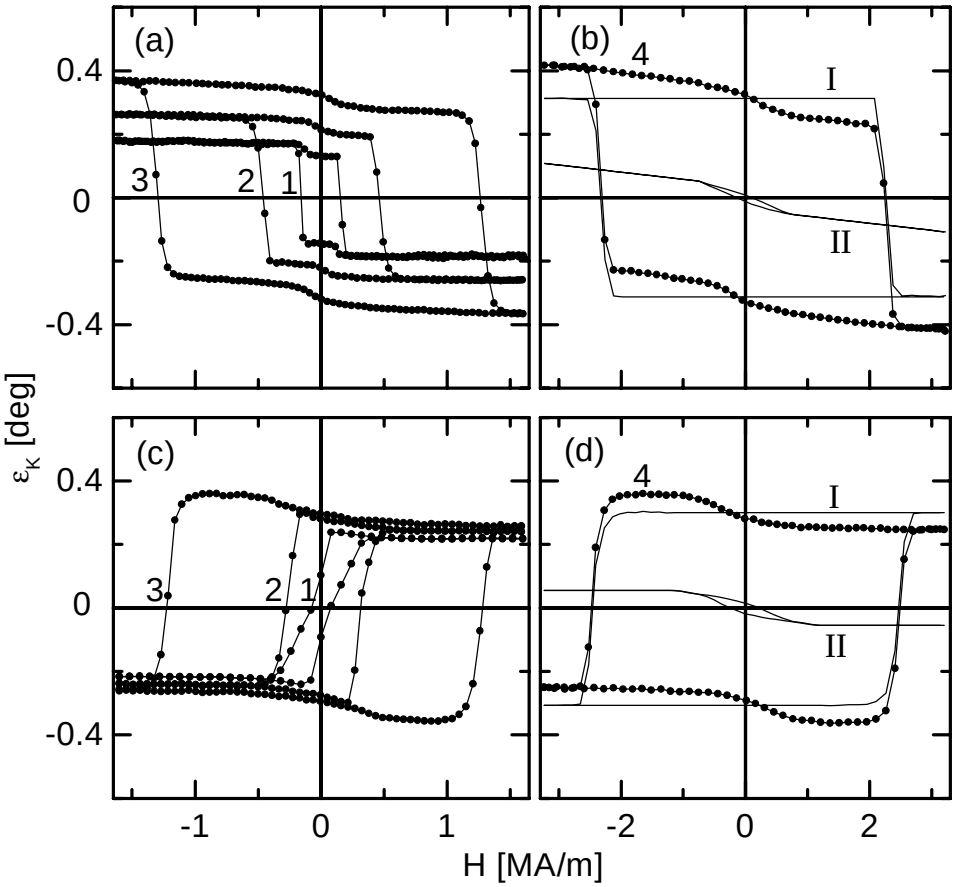

Fig. 5.3: Polar Kerr hysteresis loops of HT multilayers with t_{Fe} = 1.5 (a, b) and 3.0 nm (c, d) measured at different temperatures, 300 (1), 200 (2) 100 (3) and 50 K (4). The curves 4 are decomposed into individual components I and II (solid lines; see text).

It is interesting to follow the *T* dependencies of the individual contributions to the Kerr loops discussed above. The decomposition shown in Fig. 5.1b for *T* = RT (curves I and II) are encountered in a similar fashion at 50 K (Fig. 5.3b and d, curves I and II). Despite the different Fe modifications involved, a- and α-Fe for t_{Fe} = 1.5 (b) and 3.0 nm (d), the most prominent contributions I reveal very similar characteristics, $H_s \approx 2.2$ MA/m and $|\varepsilon^s_K| \approx 0.3°$. This clearly hints at the dominating role of the Fe/Tb interfaces. They bear a high potential of PMA in both cases which is transferred by exchange coupling to the bulk of the magnetic Fe layers irrespective of their individual structure, a- or α-Fe.

Interestingly, also the „uncoupled“ a-Fe contribution II survives in both MLs. It remains magnetically soft albeit becoming slightly hysteretic with an M_r/M_s ratio of about 0.5 and $H_c \approx$ 0.2 MA/m. Nevertheless, this latter value differs so strongly from that of the main component I that the decoupled nature of the contributions II becomes even more stringent.

At a closer look it becomes apparent that both contributions, I and II, vary differently with temperature *T*. This is evidenced by plots of ε_K^s vs. *T* in Fig. 5.4 as measured at the respective maximum field (see Fig. 5.3). In a first step the integral curves, ε_K^s vs. *T*, are decomposed into the contributions ε_K^s(I) and ε_K^s(II) vs. *T* according to the scheme demonstrated in Fig. 5.3b and d. It is seen that the uncoupled a-Fe contributions II (open circles) vary but slightly when cooling from 300 to 50 K. Both exhibit the same sign (please note that $|\varepsilon_K| = -\varepsilon_K$ is plotted in Fig. 5.4a!) and saturate smoothly at low *T*, ε_K^s(II, *T* = 50 K) ≈ -0.05 deg. These observations comply with magnetic saturation of a novel modification of a-Fe having a Curie temperature above RT in agreement with previous observations on Fe/Tb MLs containing Ag blocking layers [Kim98b].

The contributions ε_K^s(I) vs. *T* (full circles) reveal two superimposed convexly shaped contributions of the form

$$\varepsilon_K^s(T) = \varepsilon_K^s(0)(1 - T / T_C)^{\beta} \qquad (5.2)$$

with vertices at high ($T_C^{(A)} \approx$ 330 K) and intermediate temperatures ($T_C^{(B)} \approx$ 180 K). The low-*T* contribution appears much more pronounced in the case t_{Fe} = 1.5 nm. Best-fits of the data within 210 ≤ *T* ≤ 300 K (Fig. 5.4a and b, solid lines) are first used to extract the characteristics of the high-temperature phase A. We find $T_C^{(A)}$ = (322 ± 9)K for t_{Fe} = 1.5 nm. The „critical“ exponent is surprisingly small, $\beta^{(A)}$ = 0.22 ± 0.04. Similarly, we find $T_C^{(A)}$ = (346 ± 9)K and $\beta^{(A)}$ = 0.17 ± 0.02 from the data referring to t_{Fe} = 3.0 nm for 210 ≤ *T* ≤ 300 K.

It is tempting to interpret the exponents β in terms of well-known model systems. Obviously both values obtained come close to that of the two-dimensional Ising model (2dIM), β = 1/8

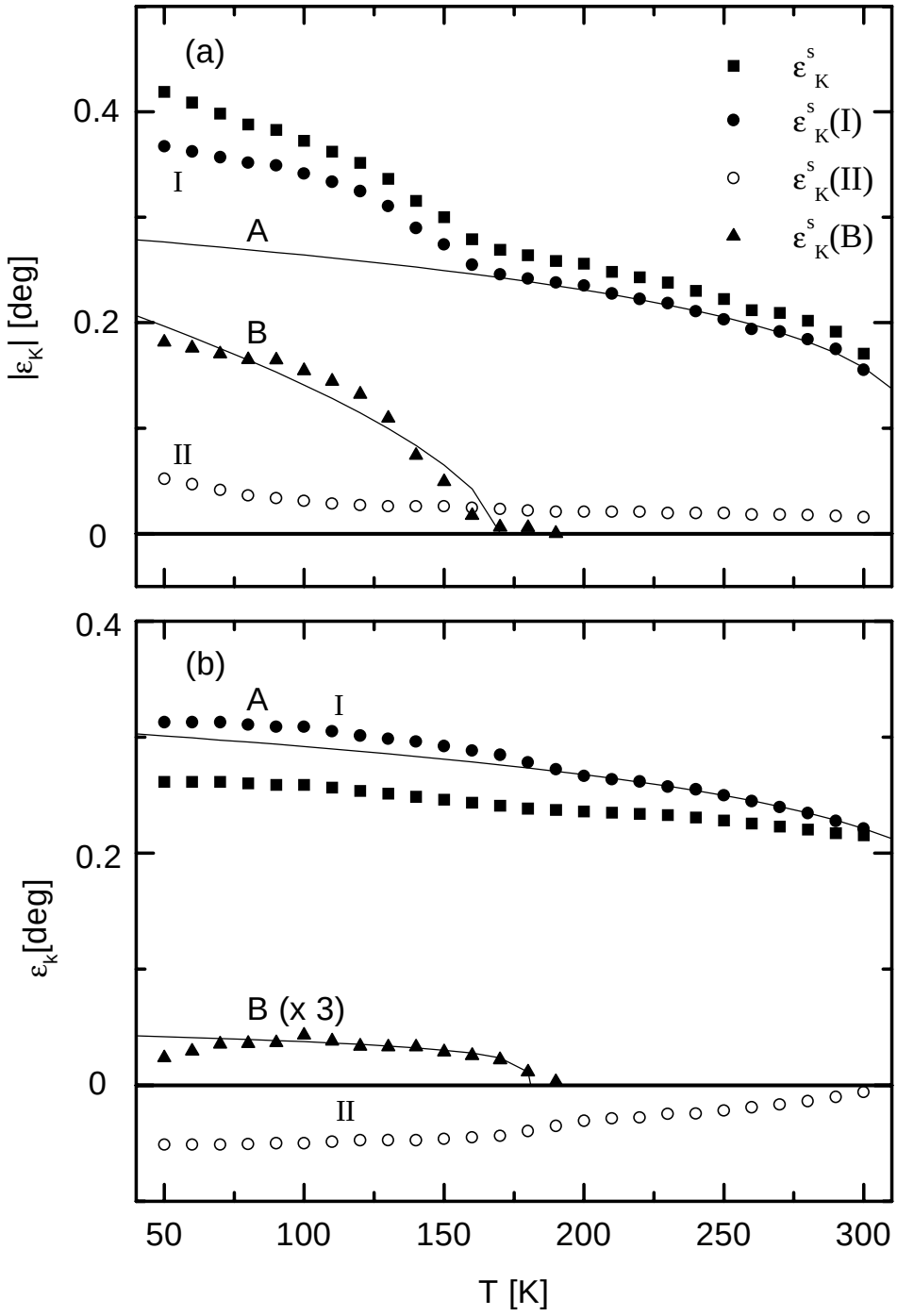

Fig. 5.4: Saturation Kerr ellipticity ε^s_K of HT multilayers with t_{Fe} = 1.5 (a) and 3.0 nm (b) measured at temperatures 50 ≤ T ≤ 300 K (solid squares). After subtraction of contributions due to isolated a-Fe, ε^s_K(II) (open circles), the data ε^s_K(I) vs. T (solid circles) are decomposed into the power-law function A (solid lines, best-fitted by Eq. (5. 2) within 210 ≤ T ≤ 300 K; see text) and ε^s_K(B) vs. T (solid triangles, best-fitted to Eq. (5. 2) by solid lines within 70 ≤ T ≤ 150 K).

[Onsa44, Yang52]. In fact, it does not seem to be unreasonable to attribute 2dIM properties to the ultrathin Fe/Tb interfaces. They refer to alloy layers of no more than about two monolayers thickness [Scho94a] and they show very strong, albeit non-infinite PMA. The following arguments might support our conjecture:

(i) The extrapolated values of $T_c \approx 330$ K lie close to that of $Fe_{0.5}Tb_{0.5}$ [Hans89]. Hence, an equimolar mixture of both components seems to govern the phase transition. This implies that either the interface is atomically smooth with Fe-Tb pairs dominating the exchange interaction, or the interface is corrugated on a depth of no more than about two monolayers. Whereas both kinds of interfaces are found in MBE grown crystalline Fe/Tb MLs, namely rough Fe-on-Tb and smooth Tb-on-Fe layers [Tapp94] only rough interfaces occur in amorphous HT MLs [Rich96a]. Moreover, Eq. (5. 1) allows us to predict the hyperfine field B_{hf} from the measured value ε_K^s (300 K) (see also Fig. 5.2c). The predicted value B_{hf} = 16.3 T compares favorably with that of an amorphous alloy $Fe_{0.5}Tb_{0.5}$, B_{hf} = 15.5 T, measured by CEMS [Ruck97] and calculated within a molecular field approach [Heim76].

(ii) It might be argued that Eq. (5. 2) will fail at some distance from T_c. Empirically, however, there are numerous examples in thin magnetic film physics, which are in favor of such a power law with a meaningful critical exponent β of the order parameter [Kohl92, Li92, Rau93]. At least the order of magnitude of the exponent β, albeit obtained outside the critical region, $|1\text{-}T/Tc| < 10^2$, can be taken as indicative of the universality class involved. In particular, assignment to any of the three-dimensional universality classes (3dIM: β = 0.325; 3d Heisenberg model: β = 0.365) [Ma76] seems safely to be ruled out.

After subtracting the high-T contributions, $\varepsilon_K^s(A)$, from $\varepsilon_K^s(I)$ vs. T we obtain the low-T contributions $\varepsilon_K^s(B)$ which may, again, be fitted to Eq. (5. 2). The following parameters emerge: $T_C^{(B)}$ = (170 ± 2)K and (180 ± 1)K, $\beta^{(B)}$ = 0.62 ± 0.08 and 0.23 ± 0.05, for t_{Fe} = 1.5 and 3.0 nm, respectively. Obviously a second component with more or less 3d ferromagnetic behavior undergoes a low-T phase transition. According to our above discussion it appears plausible to attribute these contributions to a-Fe ($T_C \approx 200$ K) [Alpe76, Rich96b], which dominates the bulk of the Fe layers when t_{Fe} = 1.5 nm, but constitutes only a small fraction when t_{Fe} = 3.0 nm. This result agrees with inferences from recent Mössbauer studies [Rich96a].

5.2.2. LT multilayers (T_s= 150 K)

One major effect of the condensation temperature T_s on the properties of Fe/Tb MLs is the difference in the critical thickness, t_{Fe}^{cr}, above which crystallization of α-Fe takes place. Whereas t_{Fe}= 3 nm suffices to yield crystallinity of the layers for T_s= 300 K, they are still amorphous in the LT case, T_s= 150 K. As discussed in Section (5.1) this situation gives rise to a rectangular hysteresis cycle with comparatively low values of both ε_K^s and $H_s = H_c$ at RT (Fig. 5.1b). Clearly strong surface-induced PMA due to exchange coupled Fe/Tb pairs [Sato86] is encountered.

However, upon cooling to below RT the Kerr-optical hysteresis loops exhibit very complex changes. This is shown for the LT ML with t_{Fe} = 3 nm in Fig. 5.5 for temperatures ranging between 250 and 160 K. Obviously the most drastic changes occur between 210 and 180 K. As will be discussed below in more detail, the observed anomalies of the ε_K vs. H curves result from two peculiarities of the a-Fe/Tb system: (i) Tb becomes ferromagnetic only below T_c = 219 K [Elli72], where it starts to dominate the magnetization of the Fe/Tb interfaces via the well-known ferrimagnetic exchange coupling, (ii) a-Fe becomes ferromagnetic below $T_c \approx$ 200 K [Alpe76, Rich96b], couples to the Fe/Tb interfaces and increasingly contributes to the Kerr ellipticity in addition to that originating from the interfaces.

A first signature of magnetic heterogeneity of our LT ML (Fig.5.5) is observed at T = 250 K, where the Kerr loop sharply bends up just before reaching the switching fields, $H_s \approx$ 0.5 MA/m. At a closer look the same feature, viz. a linear decrease of ε_K vs. H in the vicinity of H = 0, is observed with similar intensity in all Kerr loops depicted in Fig. 5.5. We are inclined to attribute this anomaly to a virtually uncoupled subsystem of a-Fe in analogy to that of the component II found in the case of the HT MLs (Fig. 5.3b and d). This contribution reveals, again, negative Kerr ellipticity. Its amplitude is virtually constant below its ordering temperature, $250 < T_c < 300$ K. Note that $T_c >$ RT is extrapolated for the HT MLs (Fig. 5.4 a and b).

Following the decomposition procedure applied to the Kerr loops shown in Fig. 5.3b and d for the HT samples we have subtracted the above discussed magneto-optic contribution II (due to uncoupled a-Fe) from some of the curves depicted in Fig. 5.5 (T = 210, 185, 180 and 160 K)

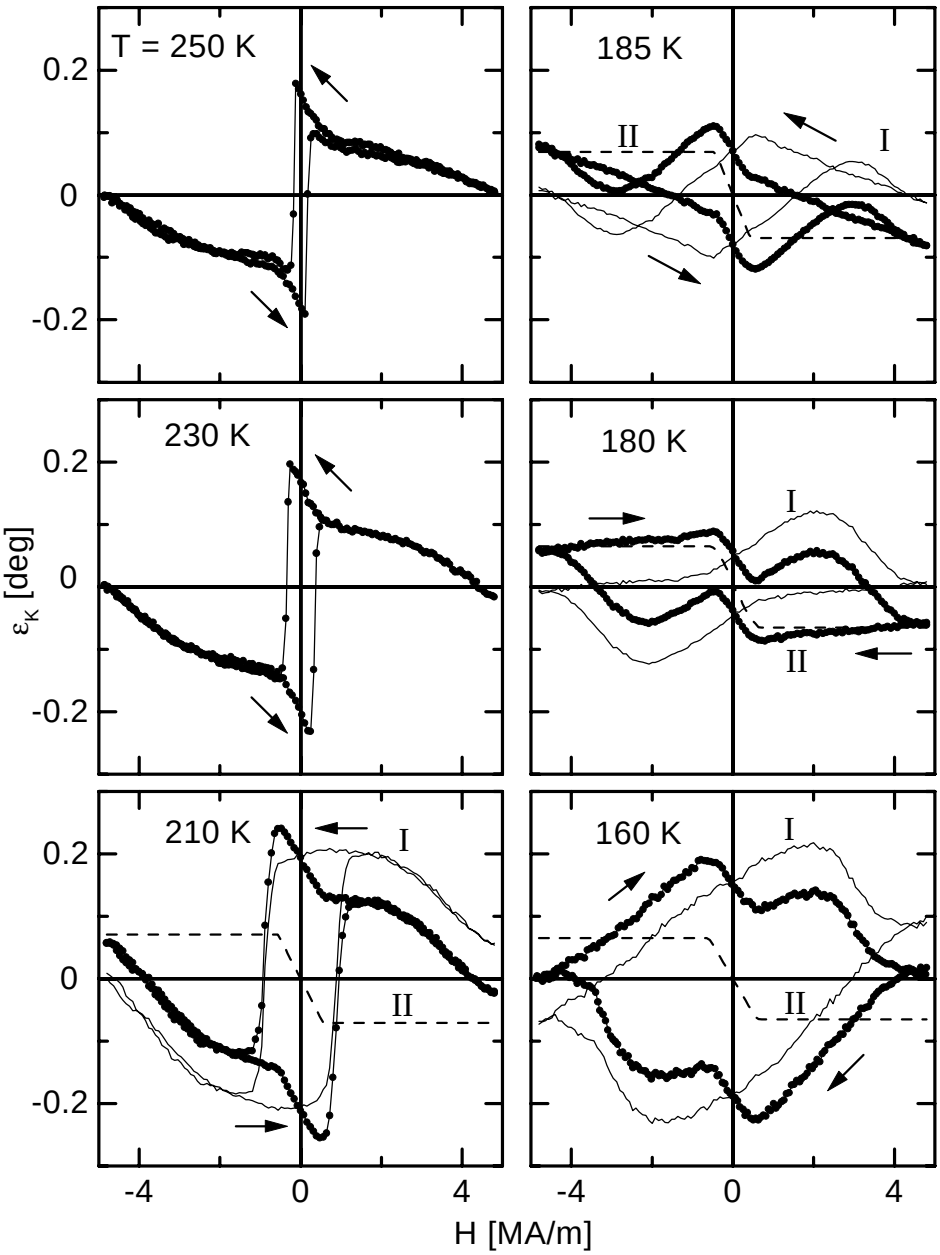

Fig. 5.5: Polar Kerr hysteresis loops of a LT multilayer with t_{Fe} = 3.0 nm measured in the direction of the arrows at different temperatures, 160 ≤ T ≤ 250 K. The curves I (thin solid lines for 210 ≥ T ≥ 160 K) refer to the measured ones (solid circles) after subtracting contributions due to isolated a-Fe (curves II, broken lines; see text).

using identical saturation values, ε_K^s = -0.15° and $H_s \approx 0.5$ MA/m. These values come close to those found for the component II in the case of the HT MLs (Fig. 5.3 and 4).

The difference curves labeled as I in Fig. 5.5 exhibit three important features: (i) the coercive field increases appreciably from $H_c \approx 1$ to 3 MA/m when cooling from 210 to 160 K; (ii) the remanence, ε_K^r, changes sign upon cooling and achieves lowest absolute values at $T \approx 180$ K; (iii) as a rule (except at $T \approx 180$ K) the saturation values ε_K^s at H = 5 MA/m are lower than the ε_K^r values. The shapes of the curves I are qualitatively interpreted under the assumption that the Kerr ellipticity signals are exclusively due to Fe, while the contributions due to Tb are neglected [see Fig. 5.2c, Chal90]. Under these conditions we argue first for the limiting cases with large positive and negative values of ε_K^r at 210 and 160 K, respectively.

At T = 210 K the large positive Kerr remanence, ε_K^r = 0.2°, proves dominance of the Fe moments in the ferrimagnetically coupled interfaces. A plot of ε_K^r vs. T in Fig. 5.6 shows a well-defined convex curvature, which can be extrapolated to higher temperatures using the

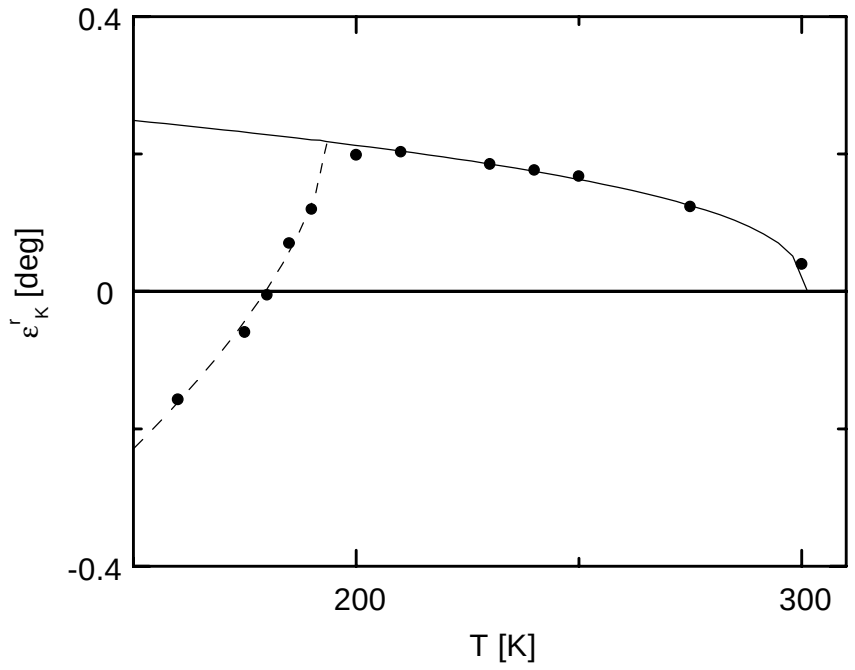

Fig. 5.6: Remanent Kerr ellipticity, ε_K^r vs. T, of a LT multilayer with t_{Fe} = 3.0 nm (see Fig. 5.5) best-fitted to Eq. (5. 2) within the range 200 ≤ T ≤ 300 K (solid line) and interpolated by a broken line below 200 K.

power law, Eq. (5. 2). Fitting the data measured between 210 and 300 K, we find a Curie temperature, T_c = 301 K. It corresponds to a Tb-rich amorphous $Fe_{0.4}Tb_{0.6}$ alloy as estimated

from magnetization data [Hans89]. This hints at an extension of the intermixed interfaces compared with the equimolar case $Fe_{0.5}Tb_{0.5}$. This seems to be typical of the LT-type quench-condensation procedure, which rules out phase segregation by thermally activated diffusion. This assertion is corroborated by the value of the best-fitted "critical" exponent, $\beta = 0.39 \pm 0.03$. It complies with 3d magnetic behavior in contrast with the result obtained for the magnetization of the much sharper HT ML interfaces (Sec. 5.2.1).

Surprisingly, the Kerr signal starts to decrease at H > 2MA/m and nearly vanishes as $H \rightarrow 5$ MA/m. Here we have to take into account the fact that we are close to the ordering temperature of Tb, $T_c = 219$ K [Elli72]. Hence, the highly susceptible Tb component becomes increasingly polarized and eventually gains Zeeman energy when being turned into the direction of H. It overcomes that of the inverted ferrimagnetically coupled Fe component, which now contributes with negative sign to ε_K. Presumably, this inversion process occurs via domain formation because of the large demagnetization fields involved and seems to saturate only above the highest field available, H = 5 MA/m. Please note that this interpretation does not account for any coupling between the individual interfaces. Exchange coupling is weak since the bulk a-Fe lacks spontaneous ordering at 210 K.

This changes drastically when lowering the temperature to $T = 160$ K, where both Tb and a-Fe are spontaneously ordered and provide full exchange coupling between the Fe/Tb interfaces. As a consequence this gives rise to a tremendous increase of the coercive force, $H_c \approx 4$ MA/m. Furthermore, dominance of Tb is now documented by the negative remanence signal, which is nearly saturated, $\varepsilon_K^r = -0.2°$. Peculiarly, however, the Kerr loop, curve I, is inclined with respect to the H axis under about 45° such that the saturated value at H = 5 MA/m becomes weakly positive. Obviously the Kerr signal becomes overcompensated by virtue of two Fe contributions revealing different orientations with respect to the magnetic field. Since the exchange coupling between Fe and Tb (T_c > 300 K) is much stronger than that between the interface parts and the bulk of the Fe layers ($T_c \approx 200$ K), probably the latter one is the first to be broken by the external field. Hence, with increasing field H the moments of the inner part of the Fe layers turn into the direction of H, whereas the Fe moments adjacent to the Tb layers stay antiparallel to both H and the Tb moments. By this mechanism, which has never been described before, we can explain the near inversion of the Kerr ellipticity at maximum field.

Much higher fields are required to break the exchange coupling within the Fe/Tb interface alloys and to achieve positive saturation.

At intermediate temperatures, $180 \leq T \leq 185$ K, the Kerr loops, curves I, reflect crossover situations. Remarkably, the Kerr remanence, ε_K^r, does not switch abruptly from +0.2° to -0.2°, as one would expect in the situation of a global compensation temperature [Reim88]. Instead, a gradual decrease of ε_K^r is encountered within a temperature interval of about 40 K as confirmed by a plot of ε_K^r vs. T in Fig. 5.6. Here the power law of the unambiguously Fe-based signal becomes gradually inverted towards negative values at $T < T_c(\mathrm{Tb}) \approx 219$ K. Unfortunately, since closed hysteresis loops are out of reach within the field range available, ε_K^r values could not be taken at $T < 160$ K, where they are eventually expected to saturate with inverted sign.

The decrease of ε_K^r strongly suggests cancellation of the global Kerr signal due to a superposition of both positive and negative contributions referring to the limiting cases discussed above. Since the Fe/Tb interfaces refer to intermixed regions with variant effective concentrations it seems plausible to assume a polydomain-like picture of the whole system, partially being strongly coupled and Tb-dominated as observed at 160 K, partially still residing in the essentially uncoupled, Fe-dominated interface situation as observed at 210 K. This view is corroborated by tentative linear superposition of the limiting cases, $\varepsilon_K(210\ \mathrm{K}) \equiv \varepsilon_h$ and $\varepsilon_K(160\ \mathrm{K}) \equiv \varepsilon_l$, in order to simulate ε_K vs. H at intermediate temperatures. Fig. 5.7 shows model functions $\varepsilon_K(185\ \mathrm{K}) = 0.45\varepsilon_h + 0.1\varepsilon_l$ and $\varepsilon_K(180\ \mathrm{K}) = 0.12\varepsilon_h + 0.4\varepsilon_l$ (solid lines) together with the corresponding experimental curves I (solid circles; Fig. 5.5). Obviously, many features of the experimental data are satisfactorily reproduced. The most conspicuous difference, the absence of sharp jumps as occurring in ε_h vs. H at $T \geq 210$ K (Fig. 5.5), is readily understood when considering multidomain processes, which give rise to sheared hysteresis loops as observed throughout the crossover range (e. g. at $T = 195$ K; see inset in Fig. 5.7a).

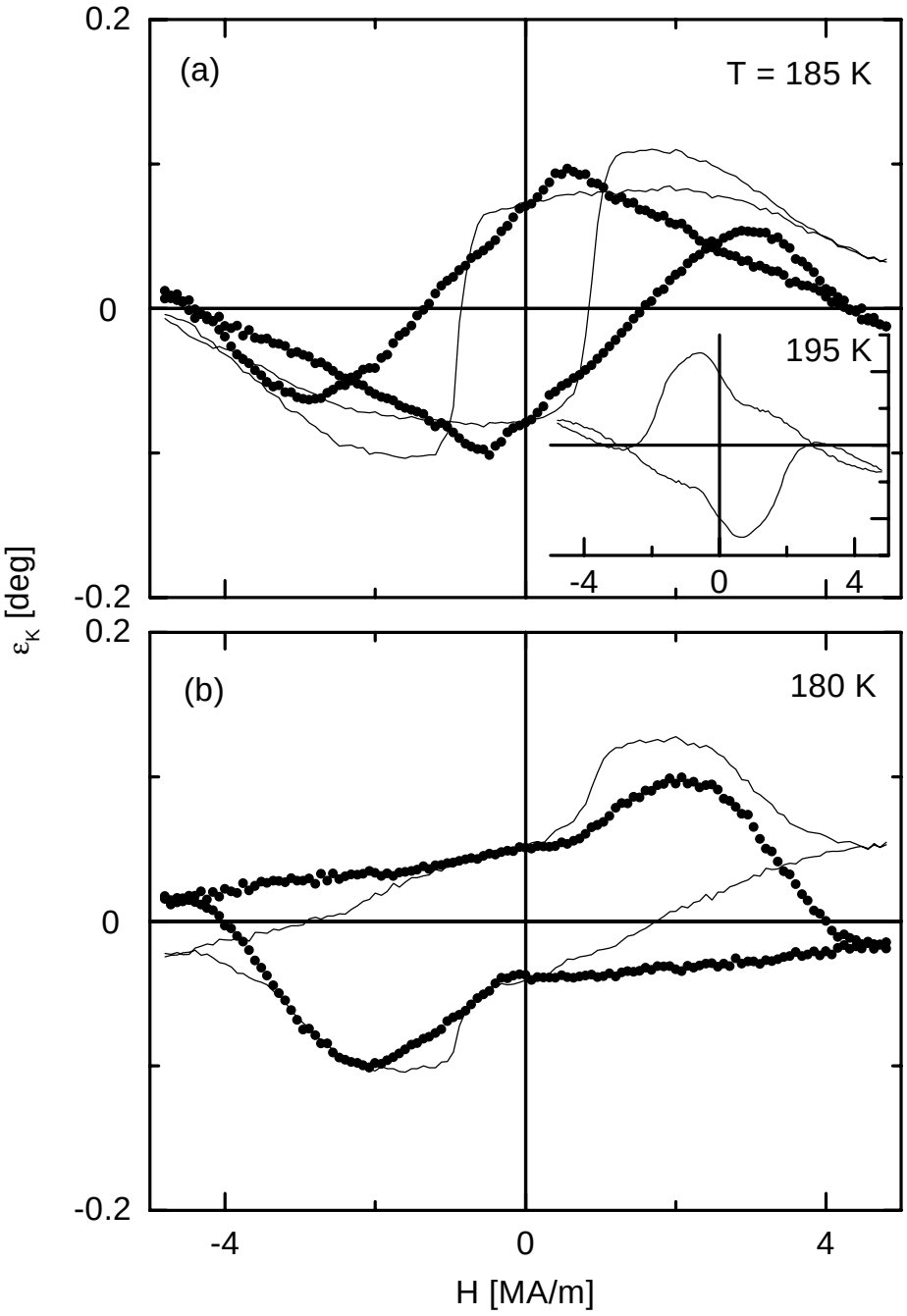

Fig. 5.7: Curves I referring to the polar Kerr hysteresis loops of a LT multilayer with t_{Fe} = 3.0 nm obtained for T = 185 K (a) and 180 K (b) (solid circles; see Fig. 5.5) and modeled by linear combination of the curves I obtained at T = 160 and 210 K (see text). Inset: Uncorrected polar Kerr hysteresis loop of a LT multilayer with t_{Fe} = 3.0 nm measured at T = 195 K.

5.2.3. Summary

It has been shown that the growing conditions of Fe/Tb MLs play an important role not only for the structure of the Fe layers, but also for the morphology and the magnetic properties of the alloyed interfaces. Obviously they are much thinner in HT MLs than in the case of LT-grown MLs. This difference seems crucial for their effective dimensionality in the temperature range T_C(a-Fe) ≈ 200 K < T < T_C(Fe/Tb) ≈ 330 K, where they can be considered as isolated magnetic subsystems. Typical 2d Ising model exponents of the magnetization, $\beta \approx 0.2$, emerge for the HT-type interfaces, whereas 3d behavior is reflected by $\beta > 0.3$ in the LT-type case. Owing to the thick interfaces encountered in LT MLs, crystallization of Fe requires substantially larger single layer thickness, t_{Fe}, than in HT MLs.

Peculiarities of the hysteresis cycles are encountered at compensation transitions of the ferrimagnetically coupled Fe/Tb system. Such a case has been realized by choosing LT conditions and t_{Fe} = 3 nm. Here the high-T dominance of Fe is replaced by Tb dominance below 200 K. In a broad crossover regime between 210 and 160 K the simultaneous growth of ferromagnetic long-range order of both Tb (T_C = 219 K) and a-Fe (T_C ≈ 200 K) gives rise to smearing of the compensation transition. This is, e. g., evidenced by the gradual change of the remnant Kerr ellipticity between +0.2° and –0.2°. In addition, two novel field-induced phenomena are reported.

(i) In the absence of exchange coupling between the interfaces at T > 210 K the Fe dominance of their magnetic moments is broken by field-induced polarization of Tb, which is close to its bulk phase transition. One observes an inversion of the magnetization curve, ε_K vs. H, in high fields.

(ii) In the presence of exchange coupling between the interfaces involving the spontaneously magnetized layers of both Tb and a-Fe at $T \approx 160$ K, the antiparallel arrangement of all Fe moments with respect to the dominating Tb moments can be broken by an external magnetic field. At H ≈ 4 MA/m one first observes decoupling of the bulk a-Fe moments from those in the interface. This causes an unusual antiparallel Fe spin arrangement with the consequence that the total magneto-optical response is nearly canceled. Higher fields, H > 5 MA/m, are required to break also the exchange coupling between Tb and Fe within the interfaces until achieving parallel alignment of all moments with the external field and to obtain maximum ε_K.

Throughout this investigation we have used the fact that the Kerr ellipticity at the photon energy used, E ≈ 2 eV, is essentially sensitive to the magnetic moment of Fe contained in the MLs. This has the advantage to follow in some detail its individual magnetic behavior.

5.3. Structural and magnetic phase diagram of Fe/Tb MLs

Structural and magnetic properties of the Fe/Tb MLs evaporated in UHV at RT will be summarized as shown in Fig. 5.8. Data were collected by means of MOKE investigations at wavelengths λ = 633 or 700 nm and at temperatures $50 \leq T \leq 300$ K on the Fe/Tb MLs with Fe and Tb thicknesses, $1.0 \leq t_{Fe} \leq 5.0$ nm and $0.7 \leq t_{Tb} \leq 2.6$ nm. They are complemented by CEMS measurements [Scho94b, Rich95], which also comprise results for t_{Tb} = 0.35 nm. Compatible results are obtained by both methods. Fig. 5.8 shows that Tb remains amorphous up to t_{Tb} = 2.6 nm, but Fe crystallizes at about t_{Fe} = 2.3 nm, t_{Fe}^{cr} = 2.3 nm, independent of Tb thickness when $t_{Tb} > 0.35$ nm. For $t_{Tb} < 0.35$ nm extremely low values of t_{Fe}^{cr} (= 1.3 nm) are encountered. This is explained by the island structure of very thin Tb films which allows the Fe layers to grow continuously over large areal fractions.

With respect to the magnetic properties of the Fe/Tb MLs the phase diagram (Fig. 5.8) can be divided into 3 categories:

(i) This category is symbolized by solid circles (●) and shows temperature independent PMA below RT. This is met in the case of a-Fe, $t_{Fe} < t_{Fe}^{cr}$ = 2.3 nm, at all Tb thicknesses investigated and in the case of thin α-Fe layers, up to about t_{Fe} = 3.5 nm, with thin Tb layers, t_{Tb} = 1.4 - 1.9 nm.

(ii) This category is symbolized by solid squares (■) and indicates the occurrence of reorientation transition from PMA at low temperatures to in-plane anisotropy at RT. In this case thick α-Fe, $t_{Fe} > 3.5$ nm, and thin α-Fe with thick Tb, $t_{Tb} > 1.9$ nm, are encountered.

(iii) This category is symbolized by solid diamonds (◆) and indicates in-plane anisotropy at all temperatures measured [Scho94b]. This occurs in α-Fe layers separated by incoherent monolayers of Tb, t_{Tb} = 0.35 nm (see above).

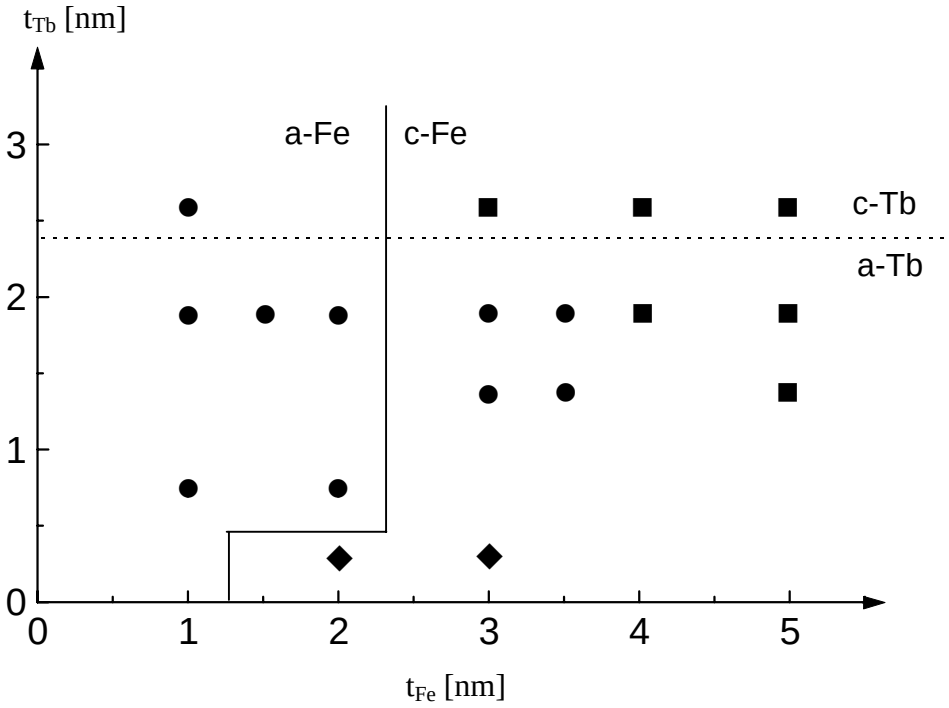

Fig. 5.8: Phase diagram of the Fe/Tb ML system ($n \geq 10$) as a function of Fe and Tb thicknesses, t_{Fe} and t_{Tb},, obtained by polar Kerr ellipticity measurements at wavelengths λ = 633 or 700 nm and at temperatures $50 \leq T \leq 300$ K on Fe/Tb MLs with $1.0 \leq t_{Fe} \leq 5.0$ nm and $0.7 \leq t_{Tb} \leq 2.6$ nm, evaporated at T = 300 K. The results for t_{Tb} = 0.35 nm refer to CEMS measurements [Scho94b]. Solid circles (●), squares (■) and diamonds (◆) denote samples with temperature-independent PMA below RT, temperature-dependent reorientation transition from PMA at low temperature to in-plane anisotropy at RT, and temperature-independent in-plane anisotropy [Scho94b], respectively. (a = amorphous, c = polycrystalline)

In the following we restrict ourselves to the categories (i) and (ii) for further investigation. In particular the samples referring to category (ii) are interesting because of their temperature driven reorientation-transition. In the case (i) it is also useful to study the change of PMA when inserting diamagnetic blocking layers like yttrium or silver.